Results in Physics 6 (2016) 1072–1079

Contents lists available at ScienceDirect

Results in Physics

journal homepage: www.journals.elsevier.com/results-in-physics

Mixed convective flow of Maxwell nanofluid past a porous vertical stretched surface – An optimal solution

M. Ramzan [a,*], M. Bilal [b], Jae Dong Chung [c], U. Farooq [d]

[a] Department of Computer Science, Bahria University, Islamabad Campus, Islamabad 44000, Pakistan
[b] Department of Mathematics, Faculty of Computing, Capital University of Science and Technology, Islamabad, Pakistan
[c] Department of Mechanical Engineering, Sejong University, Seoul 143-747, Republic of Korea
[d] Department of Mathematics, CIIT, Islamabad Campus, 44000, Pakistan

ARTICLE INFO

Article history:
Received 2 November 2016
Received in revised form 16 November 2016
Accepted 18 November 2016
Available online 23 November 2016

Keywords:
Mixed convection
Maxwell nanofluid
Soret and Dufour effects
Optimal solution
Porous medium

ABSTRACT

Present investigation is devoted to examine the mixed convective flow of Maxwell nanofluid with Soret and Dufour effects through a porous medium. Effects of variable temperature and concentration over a linearly permeable stretched surface are also taken into account. An optimal solution is obtained for the highly nonlinear set of differential equations using BVPh 2.0 Mathematica package. Graphs of different emerging pertinent parameters against velocity, temperature and concentration distributions are plotted and discussed accordingly. Numerically tabulated values of local Nusselt and Sherwood numbers are also part of this investigation. It is witnessed that concentration field is decreasing and increasing function of Brownian motion and thermophoretic parameters respectively. Further, opposite behavior of Soret number on temperature and concentration distributions is seen.

Introduction

The topic of heat transfer via porous media has been a hot subject due to its technological and engineering applications. Examples may include packed sphere beds, electro chemical processes, grain storage, insulation for buildings and lining of nuclear reactors, regeneration of heat exchangers, chemical catalytic reactors, and solar power collectors. Flagged investigations in this core area include numerous studies like Shehzad et al. [1] who examined 3D flow of Casson fluid through porous media. They carried out analysis in the presence of heat generation/absorption. Sheikholeslami et al. [2] debated flow of viscous nanofluid through a porous medium with four different nano materials and water as base fluid. Hayat et al. [3] explored influence of convective boundary conditions on magnetohydrodynamic (MHD) nanofluid flow through a porous medium over an exponentially stretching sheet using series solution technique. Makinde et al. [4] studied effects of unsteady magnetohydrodynamic, thermal radiation, chemical reaction, and thermophoresis on a vertical porous plate. They employed sixth order RK-technique accompanied by Nachtsheim and Swigert's shooting method. It was noticed that skin friction coefficient decreases and local Nusselt number increases against gradual growing values of unsteady viscosity parameter. Extensive literature is also available pertaining flows through porous medium with most recent investigations referred at [5–7].

Recent studies have given a significant attention to non-Newtonian fluid flows which are produced by stretched surfaces. The non-Newtonian flows have wide range applications in engineering including aerodynamic emission of plastic films, thinning and annealing of copper wires and liquid film condensation process etc. [8]. Unlike viscous fluids, an obvious hurdle in mathematical modelling of these fluids is that a single constitutive equation cannot exhibit all characteristics of these fluid structures. That is why several non-Newtonian fluids models have been suggested by researchers in the literature. Maxwell fluid which is a class of viscoelastic fluid, can be quoted to represent the characteristics of fluid relaxation time. Here, shear-dependent viscosity's complicated effects are excluded and allows one to focus on the influence of elasticity of fluid on boundary layer characteristics. A pioneering work by Harris [9] arguing 2D flow of upper-convected Maxwell fluid encouraged follower researchers to investigate more avenues in this direction. Sadeghy et al. [10] proposed local similarity solutions by four dissimilar approaches with the findings that velocity decreases with an increase in local Deborah number. They considered Maxwell fluid flow over a moving flat plate known as Sakiadis flow. Kumari and Nath [11] discussed numerical solution of mixed convection stagnation point Maxwell fluid flow using finite differ-

* Corresponding author.
E-mail address: mramzan@bahria.edu.pk (M. Ramzan).

http://dx.doi.org/10.1016/j.rinp.2016.11.036
2211-3797/

Nomenclature

a ,b, c	dimensional constants	Sh_x	Sherwood number
C	concentration of fluid	Sr	Soret number
c_p	specific heat	T	temperature of fluid
C_s	concentration susceptibility	T_m	mean fluid temperature
C_w	concentration on wall	T_w	wall temperature
C_∞	ambient concentration	T_∞	Ambient temperature
D_B	Brownian motion coefficient	(u, v)	velocity components
D_e	mass diffusivity	$u_w(x)$	stretching velocity along$x$ -axis
D_f	dufour number	V_0	stretching velocity along$y$ -axis
D_T	thermophoretic diffusion coeff.	(x, y)	coordinate axis
f'	dimensionless velocity	α_m	thermal diffusivity
g	gravitational acceleration	β_T	coefficient of thermal expansion
Gr_x	Grashof number	β_C	coefficient of concentration expansion
j_w	mass flux	β	Deborah number
κ	thermal conductivity	γ	porosity parameter
K_T	thermal diffusion ratio	ρ	density of fluid
K	permeability constant	λ	mixed convection parameter
Le	Lewis number	λ_1	fluid relaxation time
N	Buoyancy ratio parameter	ν	kinematic viscosity
Nb	Brownian motion parameter	ψ	stream function
Nt	thermophoresis parameter	θ	dimensionless temperature
Nu_x	Nusselt number	η	similarity variable
Pr	Prandtl number	ϕ	dimensionless concentration
q_w	surface heat flux	τ	ratio of effective heat capacity of nanoparticle and base fluid
Re_x	Reynolds number		
S	Suction parameter		

ence method. Hayat et al. [12] found series solution of stagnation point magnetohydrodynamic over a stretching surface of an upper-convected Maxwell fluid. Motivated from above works, researchers have investigated two and three dimensional Maxwell fluid flows in numerous scenarios (see Shafique et al. [13] Awais et al. [14], Nadeem et al. [15], Qayyum et al.[16], and Abbasi et al. [17]).

Nanofluids are suspended ultra fine particles in base fluids (like water and organic liquids) with a size less than 100 nm. These nanoparticles consist of metals and their oxides, therefore, they have significantly higher thermal conductivity than base fluid. Recently, carbon nanomaterials with more diverse nature industrial applications including nanotubes [18,19], carbon nanoparticles [20,21], nanofibres [22], nanowires [23] and carbon nanorods [24] have been found in various nanostructures. A novel idea of "nanofluid" in heat transfer processes presented by Choi [25] has revolutionized the modern engineering and technological world. Nanofluids have numerous applications in metallurgical and chemical sectors, transportation, production of micro-sized products, thermal therapy to cure cancer, ventilation, and air-conditioning [26]. Following this coined work, Buongiorno [27] presented a more detailed study of nanofluids highlighting salient features of thermophoresis and Brownian motion. Using proposed model of Buongiorno, Kuznetsov and Nield [28] discussed nanofluid flow past a vertical plate with convective boundary layer. Khan and Pop [29] conducted a comprehensive analysis of nanofluid flow over a stretched surface and discussed effects of thermophoresis and Brownian motion heat transfer using Keller-box numerical technique. Turkyilmazoglu [30] considering different nanoparticles like Ag, Cu, TiO_2 and Al_2O_3 examined flow of hydromagnetic viscous fluid accompanied slip condition. Makinde et al. [31] discussed numerically magneto nanofluid neighboring stagnation point in the presence of buoyancy force and convective boundary conditions using RK–method of fourth order of shooting technique. Rashidi et al. [32] debated flow of MHD nanofluid over a permeable rotating disk with discussion of entropy generation and explored that such study is really beneficial in energy conversion for mechanical systems of space vehicles with nuclear propulsion and energy generators. Mustafa et al. [33] studied nanofluid flow near a stagnation point over an exponentially stretched surface. They found the solution of the problem using Homotopy Analysis method (HAM) and MATLAB's built in bvp4c software to calculate numerical solution and found that thermophoretic impact strengthens with growth in nanoparticle volume fraction. Sheikholeslami and Ganji [34] examined Cu-water nanofluid flow between parallel plates. They used Maxwell–Garnetts and Brinkman models were to find effects of viscosity and thermal conductivity. Kuznetsov and Nield [35] reviewed flow of nanofluid through a vertical plate with convective boundary conditions and disclosed that control of nano particle fraction is passive rather than active. Afterwards, researchers have extensively investigated about two and three dimensional nanofluid structures [36–45].

To address the aforesaid subjects, need was felt to model a mathematical problem that encircle all issues and solve them with an appropriate method. Due to obvious restrictions in numerical methods [46], analytical techniques are considered as a replacement by the researchers. Amongst these, perturbation technique is most common and extensively practiced method to address a variety of engineering and science problems [47]. This tool is highly dependent on small/large parameters which is considered as a major disadvantage of this method and restricts it to handle highly nonlinear problems. To elude this constraint, non-perturbation methods like Adomian decomposition method [48] and variational iteration technique [49] were introduced. But these methods cannot guarantee series solutions' convergence. However, Liao's proposed homotopy analysis method (HAM) [50] has answered this question. This technique gives solution to highly nonlinear equations with an ample freedom to guarantee convergence of the problem. Additionally, unlike numerical methods, HAM can be applied to the problems having boundary conditions with far field characteristics. Further to HAM, Liao's newly proposed Optimal HAM [51] is a strong tool that guarantee the convergence of series solution. His idea of averaged squared residual error has led to an optimal convergence which triggered the convergence of series solution.

We here discussed the effects of Soret/Dufour and mixed convection on the flow of Maxwell nanofluid in the presence of variable temperature and concentration conditions. The proposed highly nonlinear problem is solved by using BVPh 2.0 Mathematica package [52,53] to find an optimal solution. Numerous graphs are drawn to highlight the impact of various emerging parameters against involved distributions. Numerically calculated values of local Nusselt and Sherwood numbers are shown in the form of table and are well deliberated.

Problem formulation

We assume two dimensional Maxwell nanofluid flow past a vertical stretched surface (with velocity $u_w(x)$) with variable temperature $T_w(x)$, variable concentration $C_w(x)$, uniform ambient temperature T_∞, and uniform ambient concentration C_∞ in a porous medium. We also consider amalgamated effects of Soret and Dufour with mixed convection. The buoyancy effects and density variation are also considered. Boussinesq approximation is taken for both temperature and concentration profiles (see Fig. 1). The governing equations representing the proposed model are [54]:

$$\frac{\partial u}{\partial x}+\frac{\partial v}{\partial y}=0, \tag{1}$$

$$u\frac{\partial u}{\partial x}+v\frac{\partial u}{\partial y}=\upsilon\frac{\partial^2 u}{\partial y^2}-\lambda_1\left(u^2\frac{\partial^2 u}{\partial x^2}+v^2\frac{\partial^2 u}{\partial y^2}+2uv\frac{\partial^2 u}{\partial x\partial y}\right)-\frac{\upsilon}{K}u + g[\beta_T(T-T_\infty)+\beta_C(C-C_\infty)], \tag{2}$$

$$u\frac{\partial T}{\partial x}+v\frac{\partial T}{\partial y}=\alpha_m\frac{\partial^2 T}{\partial y^2}+\frac{D_eK_T}{C_sC_p}\frac{\partial^2 C}{\partial y^2}+\tau\left[D_B\frac{\partial C}{\partial y}\frac{\partial T}{\partial y}+\frac{D_T}{T_\infty}\left(\frac{\partial T}{\partial y}\right)^2\right], \tag{3}$$

$$u\frac{\partial C}{\partial x}+v\frac{\partial C}{\partial y}=\frac{D_eK_T}{T_m}\frac{\partial^2 T}{\partial y^2}+D_B\frac{\partial^2 C}{\partial y^2}+\frac{D_T}{T_\infty}\frac{\partial^2 T}{\partial y^2}, \tag{4}$$

with appropriate boundary conditions

$$u=u_w(x)=ax,\ \ v=-V_0,\ \ T=T_w(x)=T_\infty+bx,\quad C=C_w(x)=C_\infty+cx \text{ at } y=0, \tag{5}$$

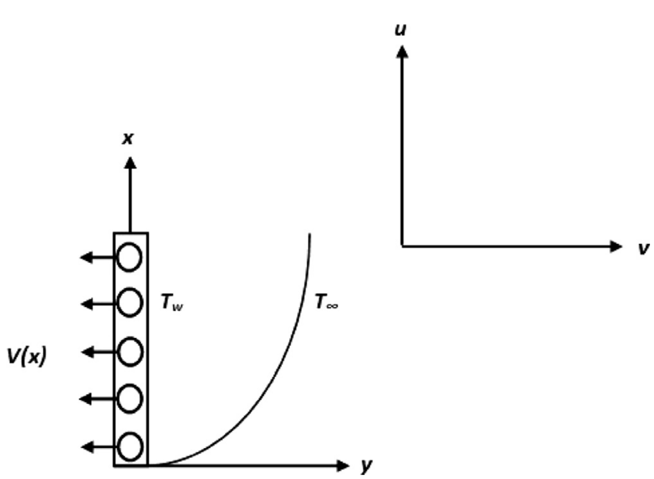

Fig. 1. Schematic flow problem.

$$u\to 0,\ \frac{\partial u}{\partial y}\to 0, T\to T_\infty,\ C\to C_\infty \text{ as } y\to\infty. \tag{6}$$

Here, velocity components u and v are along x and y-axes respectively. Also, $D_B, T\ \ , C, g, D_T, \alpha_m, \beta_T, \lambda_1,$ and $\tau=(\rho d)_p/(\rho d)_f$ are the Brownian motion coefficient, fluid temperature, nano particle concentration, gravitational acceleration, thermophoretic diffusion coefficient, thermal diffusivity, coefficient of thermal expansion, relaxation time, and the ratio of effective heat capacity of the nanoparticle to the fluid respectively. Further, $(a>0)$ and $(c>0)$ are positive constants. However, $b>0$ denotes heated plate $(T_w>T_\infty)$ and for a cooled surface $(T_w<T_\infty)$ respective constant is $b<0$. Using the following transformations [54]

$$\psi=x\sqrt{a\upsilon}f(\eta),\ \ \theta(\eta)=\frac{T-T_\infty}{T_w-T_\infty},\ \ \phi(\eta)=\frac{C-C_\infty}{C_w-C_\infty},\ \ \eta=\sqrt{\frac{a}{\nu}}y. \tag{7}$$

Satisfaction of Eq. (1) is obvious and Eqs. (2)–(6) come to the form

$$f'''+ff''-f'^2+\beta(2ff'f''-f^2f''')-\gamma f'+\lambda(\theta+N\phi)=0, \tag{8}$$

$$\frac{1}{Pr}\theta''+f\theta'-\theta f'+D_f\phi''+Nb\theta'\phi'+Nt\theta'^2=0, \tag{9}$$

$$\phi''+PrLe(f\phi'-\phi f')+SrLe\theta''+\frac{Nt}{Nb}\theta''=0, \tag{10}$$

$$f(0)=S,\ f'(0)=1,\ \theta(0)=1,\ \phi(0)=1, \tag{11}$$

$$f'(\infty)\to 0,\ f''(\infty)\to 0,\ \theta(\infty)\to 0,\ \phi(\infty)\to 0, \tag{12}$$

with Nt, $Le=\alpha_m/D_B$, Nb, D_f, $Pr=\upsilon/\alpha_m$, $\lambda, \beta(\geqslant 0)$, N, γ, and Sr are thermophoresis parameter, Lewis number, Brownian motion parameter, Dufour number, Prandtl number, dimensionless mixed convection parameter, Deborah number, dimensionless concentration buoyancy parameter, dimensionless porosity parameter, and Soret number respectively. Defining these parameters

$$\begin{aligned}&\lambda=\tfrac{g\beta_Tb}{a^2}=\tfrac{g\beta_T(T_w-T_\infty)x^3/\upsilon^2}{u_w^2x^2/\upsilon^2}=\tfrac{Gr_x}{Re_x^2},\ \ N=\tfrac{\beta_C(C_w-C_\infty)}{\beta_T(T_w-T_\infty)},\\&\gamma=\tfrac{\upsilon}{aK},\ \ \beta=a\lambda_1,\ \ D_f=\tfrac{D_eK_T(C_w-C_\infty)}{C_sC_p(T_w-T_\infty)\upsilon},\\&Sr=\tfrac{D_eK_T(T_w-T_\infty)}{T_m\alpha_m(C_w-C_\infty)},\ \ Nb=\tfrac{(\rho d)_pD_B(C_w-C_\infty)}{(\rho d)_f\upsilon},\ \ Nt=\tfrac{(\rho d)_pD_T(T_w-T_\infty)}{(\rho d)_fT_\infty\upsilon}.\end{aligned} \tag{13}$$

Here, $Re_x=u_wx/\nu$, $Gr_x=g\beta_T(T_w-T_\infty)x^3/\upsilon^2$ are the local Reynolds and Grashof numbers. Moreover, $\lambda>0, \lambda<0,$ and $\lambda=0$ depict supporting flow (heated plate), opposing flow (cooled plate) and forced convection flow. Moreover, Ncan take positive values $(N>0)$ and negative values $(N<0)$ with $N=0$ (in the absence of mass transfer). The local Nusselt and Sherwood numbers are symbolized by:

$$Nu_x=\frac{xq_w}{k(T_w-T_\infty)},\ \ Sh_x=\frac{xj_w}{D_B(C_w-C_\infty)}, \tag{14}$$

where q_w and j_w are represented by

$$q_w=-k\left(\frac{\partial T}{\partial y}\right)_{y=0},\ j_w=-D_B\left(\frac{\partial C}{\partial y}\right)_{y=0}. \tag{15}$$

In non-dimensional, local Nusselt, and Sherwood numbers are presented as

$$Re_x^{-1/2}Nu_x=-\theta'(0),\ \ Re_x^{-1/2}Sh_x=-\phi'(0). \tag{16}$$

Series solution development

Here, we intend to interpret the convergence of the series solutions by renowned Optimal Homotopy analysis method (OHAM)

[50,52]. The initial estimates and the respective operators are required for the homotopic solutions. For the present flow, these are depicted as follows:

$$f_0(\eta) = S + 1 - exp(-\eta),\ \theta_0(\eta) = exp(-\eta),\ \phi_0(\eta) = exp(-\eta), \tag{17}$$

and

$$L_f = \frac{d^3f}{d\eta^3} - \frac{df}{d\eta},\ L_\theta = \frac{d^2\theta}{d\eta^2} - \theta,\ L_\phi = \frac{d^2\phi}{d\eta^2} - \phi. \tag{18}$$

Following the foot steps given in [50]. The general solutions of Eqs. (8)–(10) are given by

$$f_m(\eta) = f_m^*(\eta) + C_1 + C_2 exp(\eta) + C_3 exp(-\eta), \tag{19}$$

$$\theta_m(\eta) = \theta_m^*(\eta) + C_4 exp(\eta) + C_5 exp(-\eta), \tag{20}$$

$$\phi_m(\eta) = \phi_m^*(\eta) + C_6 exp(\eta) + C_7 exp(-\eta), \tag{21}$$

where $f_m^*(\eta), \theta_m^*(\eta)$ and $\phi_m^*(\eta)$ represent the special solutions and

$$C_2 = C_4 = C_6 = 0,\ C_1 = -C_3 - f_m^*(0),$$

$$C_3 = \left.\frac{\partial f_m^*(\eta)}{\partial \eta}\right|_{\eta=0},\ C_5 = -\theta_m^*(0),\ C_7 = -\phi_m^*(0), \tag{22}$$

with C_i $(i = 1 - 7)$ are the arbitrary constants.

Optimal solution

As suggested by Liao [51], averaged squared residual errors that can result in excellent approximations of optimal convergence control parameters are assumed to be:

$$\epsilon_m^f = \frac{1}{k+1}\sum_{j=0}^{k}\left[N_f\left(\sum_{i=0}^{m}\widehat{f}(\eta), \sum_{i=0}^{m}\widehat{\theta}(\eta), \sum_{i=0}^{m}\widehat{\phi}(\eta)\right)_{\eta=j\delta\eta}\right]^2 .d\eta, \tag{23}$$

$$\epsilon_m^\theta = \frac{1}{k+1}\sum_{j=0}^{k}\left[N_\theta\left(\sum_{i=0}^{m}\widehat{f}(\eta), \sum_{i=0}^{m}\widehat{\theta}(\eta), \sum_{i=0}^{m}\widehat{\phi}(\eta)\right)_{\eta=j\delta\eta}\right]^2 .d\eta, \tag{24}$$

$$\epsilon_m^\phi = \frac{1}{k+1}\sum_{j=0}^{k}\left[N_\phi\left(\sum_{i=0}^{m}\widehat{f}(\eta), \sum_{i=0}^{m}\widehat{\theta}(\eta), \sum_{i=0}^{m}\widehat{\phi}(\eta)\right)_{\eta=j\delta\eta}\right]^2 .d\eta, \tag{25}$$

where k is an integer. The overall squared residual error ϵ_m^t is given by

$$\epsilon_m^t = \epsilon_m^f + \epsilon_m^\theta + \epsilon_m^\phi, \tag{26}$$

with $\delta\eta = 0.5$, and $k = 20$. Mathematica BVPh 2.0 package is used to minimize these errors. At 3^{rd} order of approximation, the values of optimal convergent control parameters are $\hbar_f = -0.75293$, $\hbar_\theta = -0.90738$ and $\hbar_\phi = -0.933951$ with total averaged squared error $\epsilon_m^t = 0.000141212$. At 3^{rd} order of approximation with $S = 0.5,\ \gamma = \lambda = \Pr = Le = N = 1,\ Sr = 0.2,\ Nt = Df = \beta = 0.1,$ and $Nb = 0.8$, the values of averaged squared residual errors are given in Table 1. It can be observed that increasing values of higher order of approximations results in decrease in averaged squared residual errors. Fig. 2 is portrays the propensity of average squared residual error $Co = (\hbar_f = \hbar_\theta = \hbar_\phi)$ versus an optimal value of all three auxiliary control parameters $\hbar_f$, $\hbar_\theta$ and $\hbar_\phi$ at 2^{nd}, 4^{th} and 6^{th} iterations using Mathematica package BVPh 2.0. It can be perceived that increasing values of order of iterations give rise to optimal convergence control parameters to a -0.67 converging value.

Table 1
Averaged squared residual errors for varied order of approximations.

m	ϵ_m^f	ϵ_m^θ	ϵ_m^ϕ
2	5.79×10^{-4}	1.48×10^{-4}	7.14×10^{-4}
6	1.42×10^{-4}	4.05×10^{-6}	7.05×10^{-6}
10	2.10×10^{-5}	8.18×10^{-7}	3.70×10^{-6}
16	1.41×10^{-5}	6.30×10^{-8}	3.09×10^{-6}
20	1.07×10^{-5}	1.42×10^{-12}	2.82×10^{-6}
26	1.06×10^{-5}	5.26×10^{-14}	2.66×10^{-6}
30	1.01×10^{-5}	1.24×10^{-16}	1.33×10^{-6}

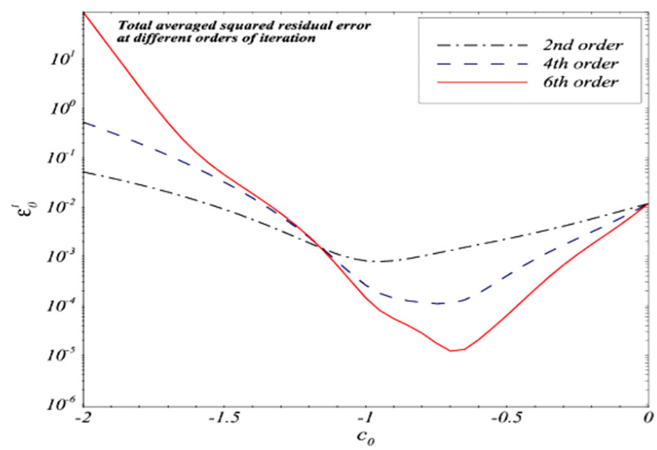

Fig. 2. Minimum averaged squared residual errors for 2nd, 4th, and 6th order of approximations.

Results and discussion

The purpose of this section is to deliberate the significant characteristics of promising parameters on velocity, temperature, and nanoparticle concentration profiles. Fig. 3 portrays the impact of suction parameter S on the velocity profile. It is witnessed that velocity field is diminishing function of S. Impact of Deborah number β on the velocity distribution is given in Fig. 4. It is noticed that velocity profile is a waning function of Deborah number. The effect of porosity parameter γ on velocity field is depicted in Fig. 5. It is witnessed that velocity distribution is dwindling function of porosity parameter. Physically, an increase in resistance against the fluid flow is observed by increasing thickness of porous medium which results in decrease in fluid velocity. Fig. 6 shows the assisting flow $(\lambda > 0)$ which speed up the fluid's flow for positive gravitational

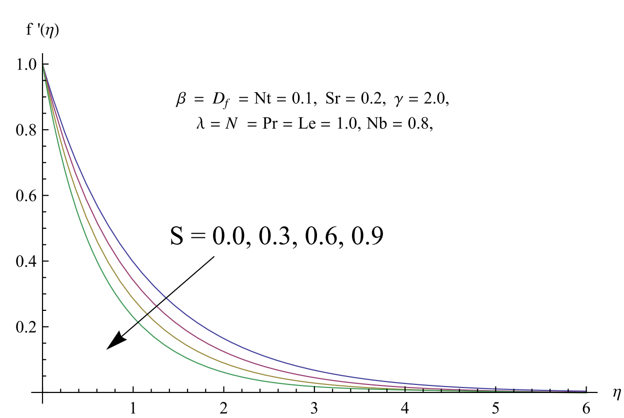

Fig. 3. Effect of S on $f'(\eta)$.

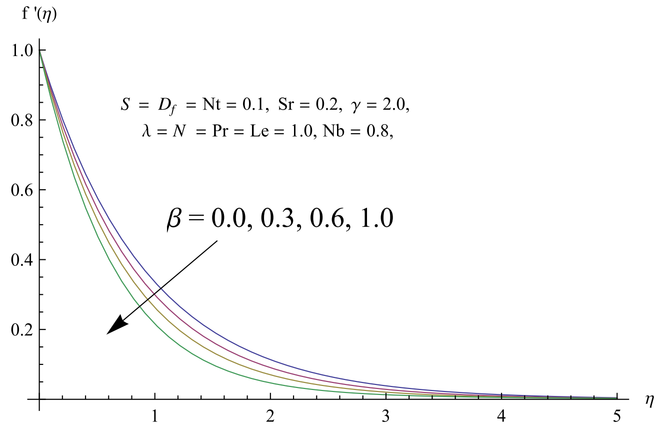

Fig. 4. Effect of β on $f'(\eta)$.

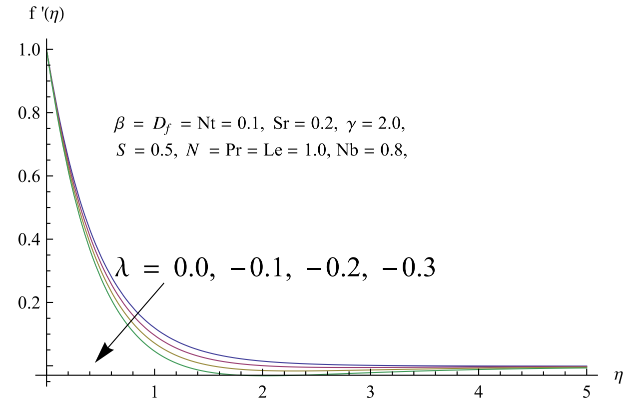

Fig. 7. Effect of $\lambda < 0$ on $f'(\eta)$.

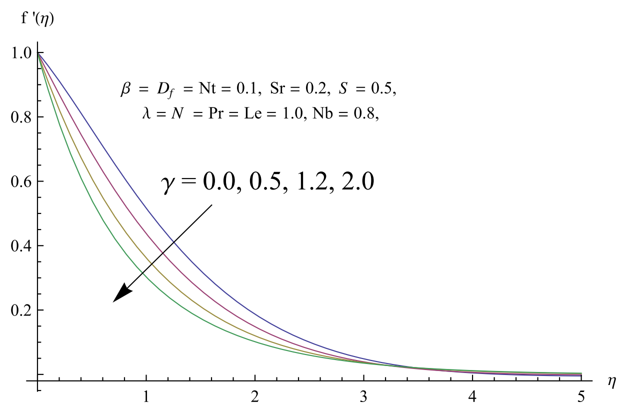

Fig. 5. Effect of γ on $f'(\eta)$.

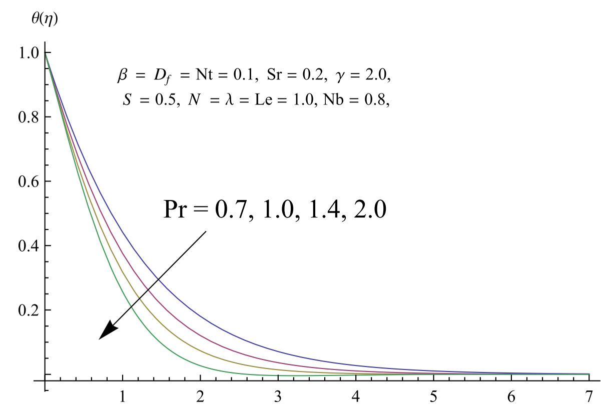

Fig. 8. Influence of *Pr* on $\theta(\eta)$.

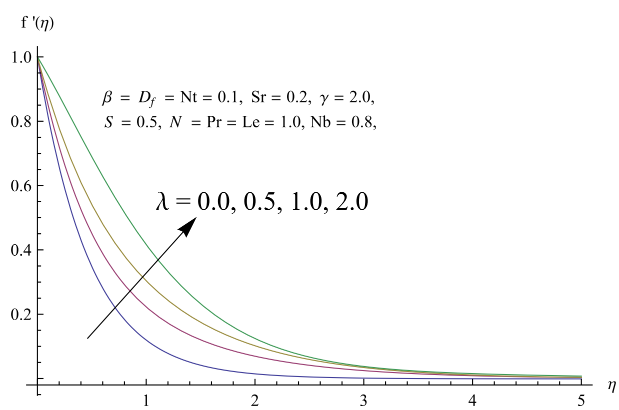

Fig. 6. Effect of $\lambda > 0$ on $f'(\eta)$.

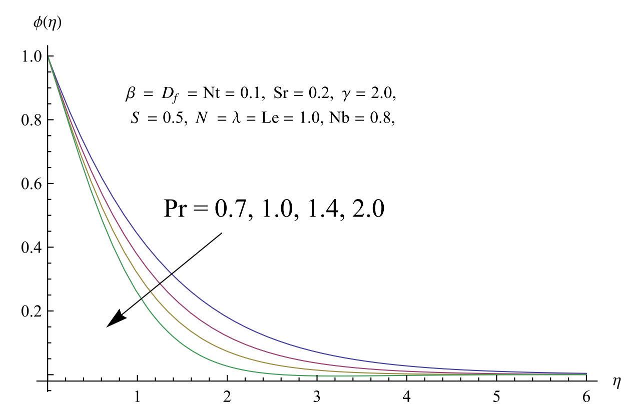

Fig. 9. Influence of *Pr* on $\phi(\eta)$.

force and hence results in an increase in fluid's velocity. On the other hand, Fig. 7 depicts the opposing flow ($\lambda < 0$) which resists the fluid's flow. In Figs. 8 and 9, we observe the effect of *Pr* on temperature profile $\theta(\eta)$ and nanoparticle concentration profile $\phi(\eta)$. Increasing values of Prandtl number cause an attenuation in both temperature and nanoparticle concentration distributions. This is because of the fact that a feebler thermal diffusivity is witnessed for higher Prandtl number. Figs. 10 and 11 exhibit the effect of the Dufour number *Df* on $\theta(\eta)$ and $\phi(\eta)$. It is found that temperature and concentration profiles increase and decrease respectively versus increasing values of Dufour number. Higher values of Dufour number lower temperature and ultimately larger temperature distribution is observed. On the contrary, an opposite behavior is witnessed in case of concentration field. Figs. 12 and 13 illustrate that the Soret number *Sr* decreases temperature profile while there is an increase in concentration profile and boundary layer thickness. Higher temperature difference and a lower concentration difference are observed because of increasing values of the Soret number. This variation in the temperature and concentration differences is liable for the decrease in the temperature and an

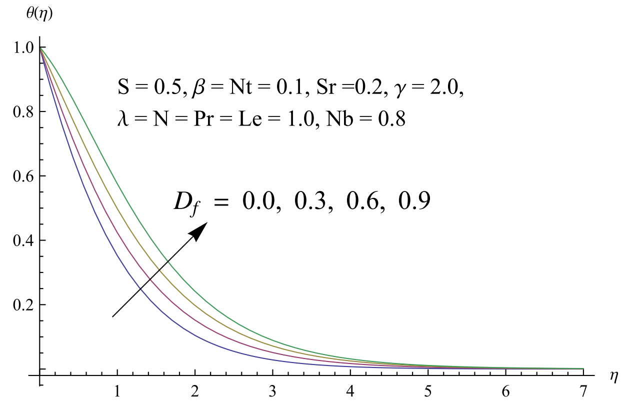

Fig. 10. Influence of D_f on $\theta(\eta)$.

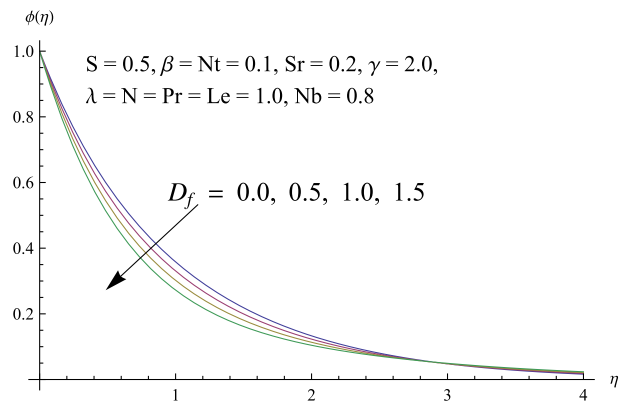

Fig. 11. Influence of D_f on $\phi(\eta)$.

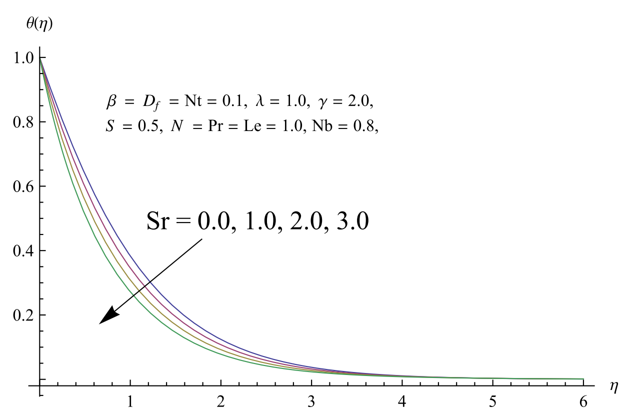

Fig. 12. Influence of Sr on $\theta(\eta)$.

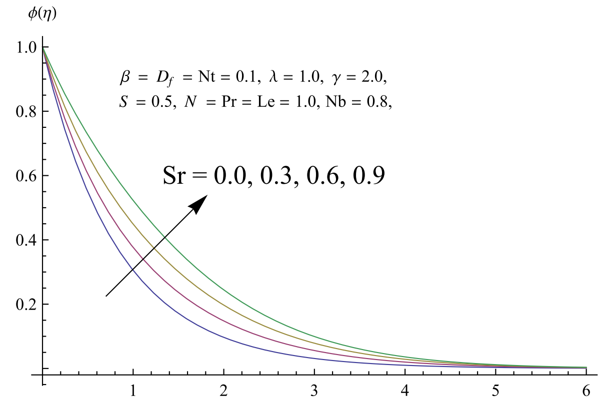

Fig. 13. Influence of Sr on $\phi(\eta)$.

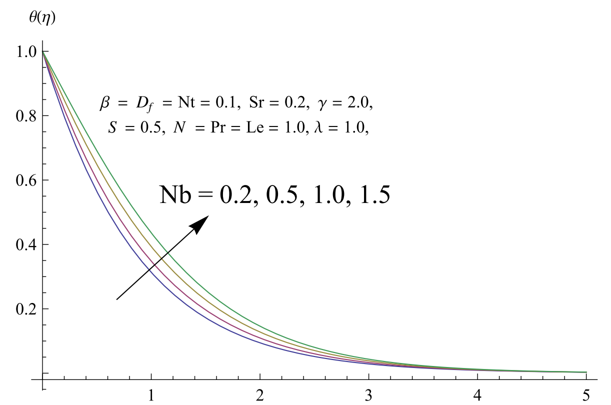

Fig. 14. Influence of Nb on $\theta(\eta)$.

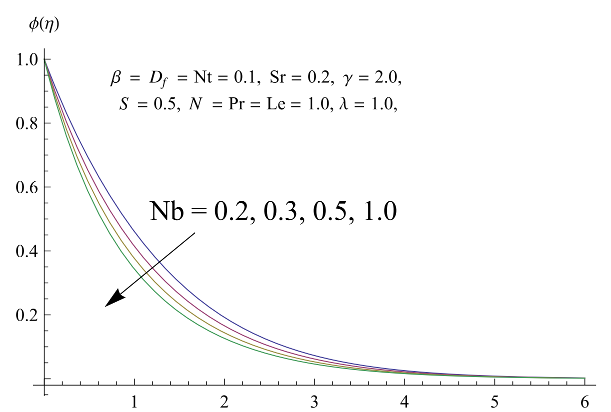

Fig. 15. Influence of Nb on $\phi(\eta)$.

increase in the concentration. It is also noticed that the Dufour and Soret numbers have fairly contrary effects for temperature and nanoparticle concentration fields. The consequences of Brownian motion parameter Nb on temperature and concentration distribution are depicted in Figs. 14 and 15. It is examined that temperature profile is larger for higher values of Brownian motion parameter. An increase in Brownian motion parameter Nb amplify the random motion of the fluid particles which produces more heat and reduces the concentration of the fluid. Figs. 16 and 17 demonstrate the influence of thermophoresis parameter Nt on temperature and nanoparticle concentration fields. It is perceived that with an increase in thermophoresis parameter both the temperature profile and thermal boundary layer thickness also increase. It is also shown that this enhancement in thermophoresis parameter pushes the nanoparticles away from the hot surface which results in an increase in volume fraction distribution.

A comparison in the limiting case is presented in Table 2, where a very good agreement is observed for the Nusselt number when different values of suction/injection parameter and Prandtl number are considered.

Table 3(a) and 3(b) show the values of the local Nusselt number $Nu_x Re_x^{-1/2}$ and the local Sherwood number $ShRe_x^{-1/2}$. The magnitude of the local Nusselt number increases for S, λ, N, Pr and Sr. However, it decreases for values of Nb, β, Df, γ, Le, and Nt. The magni-

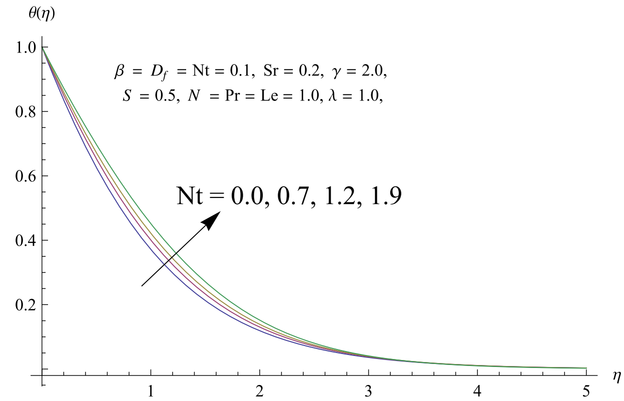

Fig. 16. Influence of Nt on $\theta(\eta)$.

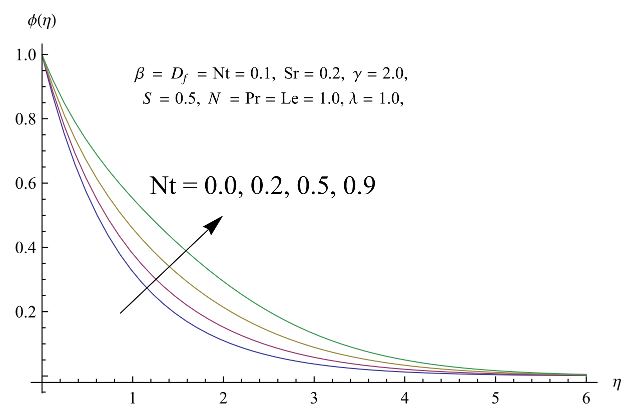

Fig. 17. Influence of Nt on $\phi(\eta)$.

Table 2
Comparison of $-\theta'(0)$ for some values of Pr and S when $\beta = \gamma = \lambda = D_f = Nb = Nt = \phi = 0$.

S	Pr	Ishak et al. [55]	Hayat et al. [56]	Present
−1.5	0.72	0.4570	0.4570273	0.4570271
	1	0.5000	0.5000000	0.5000000
	10	0.6542	0.6451648	0.6451645
0	0.72	0.8086	0.8086314	0.8086313
	1	1.0000	1.0000000	1.0000000
	3	1.9237	1.92359132	1.9359130
	1.0	3.7207	3.7215968	3.7215958
1.5	0.72	1.4944	1.4943687	1.4943680
	1	2.0000	2.0000621	2.0000620
	10	16.0842	16.096248	16.096232

tude of local Sherwood number decreases for increasing values of β, γ, Sr and Nt whereas it increases for large values of Df, S, N, Pr, λ, Nb, and Le.

Conclusions

It is of great interest in this exploration to examine effects of mixed convection, Soret and Dufour past a permeable medium of Maxwell nanofluid flow. Effects of variable temperature and concentration over a linearly porous stretched surface are also taken into account. An optimal solution is obtained for the highly nonlinear set of differential equations using BVPh 2.0 Mathematica package. Consideration of the problem along with its proposed solution is unique and has been not discussed in the literature before. The significant findings of the present study are listed below:

- Nanoparticle concentration distribution is a decreasing and increasing function of Nb and Nt.
- Velocity distribution reduces with an increase in values of S.
- θ and ϕ decrease with growing values of Pr.
- The impact of Df on θ and ϕ are opposite.
- Local Nusselt and Sherwood numbers are larger for increasing values of S and λ.

Table 3(a)
Local Nusselt number $Nu_x Re_x^{-1/2}$ and the local Sherwood number $ShRe_x^{-1/2}$ against values of γ, λ, N, S, β and Pr when $Df = 0.1$, $Le = 1$, $Sr = 0.2$, $Nb = 0.8$ and $Nt = 0.1$ are fixed.

S	β	γ	λ	N	Pr	$-\theta'(0)$	$-\phi'(0)$
0.0	0.1	2.0	1.0	1.0	1.0	0.71104	0.89301
0.3						0.79696	1.01679
0.5						0.85983	1.10661
0.9						0.99873	1.30359
0.5	0.0					0.86690	1.11816
	0.2					0.85263	1.09559
	0.4					0.83795	1.07326
	0.1	0.5				0.91493	1.19556
		1.0				0.89498	1.16286
		1.5				0.87680	1.13337
		2.0	0.5			0.81772	1.03883
			0.8			0.84445	1.08202
			1.2			0.87379	1.12906
			1.0	−0.2		0.80842	1.02316
				−0.1		0.81357	1.03149
				0.5		0.84071	1.07596
				1.0	0.7	0.77431	0.84566
					1.2	0.88622	1.27852
					1.5	0.89045	1.53416

Table 3(b)
Local Nusselt number $Nu_x Re_x^{-1/2}$ and the local Sherwood number $ShRe_x^{-1/2}$ against values of Sr, Nb, Df, Le, and Nt when $S = 0.5$, $\beta = 0.1$, $\gamma = 2.0$, $\lambda = N = Pr = 1.0$ are fixed.

Df	Le	Sr	Nb	Nt	$-\theta'(0)$	$-\phi'(0)$
0.0	1.0	0.2	0.8	0.1	0.92430	1.08556
0.2					0.79244	1.12890
0.4					0.64798	1.17570
0.1	0.7				0.93603	0.82755
	1.2				0.81957	1.28184
	1.5				0.76852	1.53285
	1.0	0.0			0.82745	1.21843
		0.1			0.84341	1.16386
		0.4			0.89416	0.98468
		0.2			0.95038	0.77806
			0.3		1.07399	0.89003
			0.5		0.97908	1.02149
			1.0		0.78921	1.14098
			0.8	0.0	0.87116	1.17100
				0.3	0.83699	0.98765
				0.5	0.81388	0.88051

Competing interests

The authors have not any competing interests in the manuscript.

Acknowledgement

This research is supported by Korea Institute of Energy Technology Evaluation and Planning (KETEP) granted financial resource from the Ministry of Trade, Industry & Energy of Korea (No. 20132010101780).

References

[1] Shehzad SA, Hayat T, Alsaedi A. Three-dimensional MHD flow of Casson fluid in porous medium with heat generation. J Appl Fluid Mech 2016;9(1):215–23.
[2] Sheikholeslami M, Ellahi R, Ashorynejad HR, Domairry G, Hayat T. Effects of heat transfer in flow of nanofluids over a permeable stretching wall in a porous medium. J Comput Theor Nanosci 2014;11(2):486–96.
[3] Hayat T, Imtiaz M, Alsaedi A, Mansoor R. MHD flow of nanofluids over an exponentially stretching sheet in a porous medium with convective boundary conditions. Chin Phys B 2014;23(5):054701.
[4] Makinde OD, Khan WA, Culham JA. MHD variable viscosity reacting flow over a convectively heated plate in a porous medium with thermophoresis and radiative heat transfer. Int J Heat Mass Transf 2016;93:595–604.
[5] Ellahi R, Hassan M, Zeeshan A. Shape effects of nanosize particles in Cu—H_2O nanofluid on entropy generation. Int J Heat Mass Transf 2015;81:449–56.
[6] Ramesh K. Influence of heat and mass transfer on peristaltic flow of a couple stress fluid through porous medium in the presence of inclined magnetic field in an inclined asymmetric channel. J Mol Liq 2016;219:256–71.
[7] Ahmad M, Ahmad I, Sajid M. Magnetohydrodynamic time-dependent three-dimensional flow of Maxwell fluid over a stretching surface through porous space with variable thermal conditions. J Braz Soc Mech Sci 2016;1–12.
[8] Turkyilmazoglu M, Pop I. Exact analytical solutions for the flow and heat transfer near the stagnation point on a stretching/shrinking sheet in a Jeffrey fluid. Int J Heat Mass Transf 2013;57:82–8.
[9] Harris J. Rheology and non-newtonian flow. London: Longman; 1977.
[10] Sadeghy K, Najafi AH, Saffaripour M. Sakiadis flow of an upper-convected Maxwell fluid. Int J Non Linear Mech 2005;40:1220–8.
[11] Kumari M, Nath G. Steady mixed convection stagnation-point flow of upper convected Maxwell fluids with magnetic field. Int J Non Linear Mech 2009;44:1048–55.
[12] Hayat T, Abbas Z, Sajid M. MHD stagnation-point flow of an upper-convected Maxwell fluid over a stretching surface. Chaos Solitons Fract 2009;39:840–8.
[13] Shafique Z, Mustafa M, Mushtaq A. Boundary layer flow of Maxwell fluid in rotating frame with binary chemical reaction and activation energy. Results Phys 2016;6:627–33.
[14] Awais M, Hayat T, Irum S, Alsaedi A. Heat generation/absorption effects in a boundary layer stretched flow of Maxwell nanofluid; Analytic and Numeric solutions. PLoS ONE 2015;10(6):e0129814.
[15] Nadeem S, Haq R, Khan ZH. Numerical study of MHD boundary layer flow of a Maxwell fluid past a stretching sheet in the presence of nanoparticles. J Taiwan Inst Chem Eng 2014;45:121–6.
[16] Qayyum A, Hayat T, Alhuthali MS, Malaikah H. M, Newtonian heating effects in three-dimensional flow of viscoelastic fluid. Chin Phys B 2014;23:054703.
[17] Abbasi FM, Mustafa M, Shehzad SA, Alhuthali MS, Hayat T. Analytical study of Cattaneo-Christov heat flux model for a boundary layer flow of Oldroyd-B fluid. Chin Phys B 2015;25(1):014701.
[18] Hu GJ, Cao BY, Guo ZY. Molecular dynamics studies on thermal transport through multiwalled carbon nanotubes. J Nanosci Nanotech 2015;15:2989–96.
[19] Ellahi R, Hassan M, Zeeshan A. Study of natural convection MHD nanofluid by means of single and multiwalled carbon nanotubes suspended in a salt water solution. IEEE Trans Nanotech 2015. doi: http://dx.doi.org/10.1109/TNANO.2015.2435899.
[20] Yu J, Ahn J, Zhang Q, Yoon SF, Rusli, Li YJ, Gan B, Chew K, Tan KH. Catalyzed growth of carbon nanoparticles by microwave plasma chemical vapor deposition and their field emission properties. J Appl Phys 2002;91:433–6.
[21] Akbar NS, Raza M, Ellahi R. Impulsion of induced magnetic field for Brownian motion of nanoparticles in peristalsis. Appl NanoSci 2016;6(3):359–70.
[22] Chen Y, Patel S, Ye YG, Shaw ST, Luo LP. Field emission from aligned high-density graphitic nanofibers. Appl Phys Lett 1998;73:2119–21.
[23] Cocoletzi GH, Takeuchi N. First principles calculations of the structural and electronic properties of zinc sulfide nanowires. Quantum Matter 2013;2:382–7.
[24] Tüzün B, Erkoç S. Structural and electronic properties of unusual carbon nanorods. Quantum Matter 2012;1:136–48.
[25] Choi SUS. Enhancing thermal conductivity of fluids with nanoparticles. Proceeding of ASME Int. Mech. Eng. Congr. Expo, vol. 66.
[26] Wong KV, Leon OD. Applications of nanofluids: current and future. Adv Mech Eng 2010. 519659.
[27] Buongiorno J. Convective transport in nanofluids. ASME J Heat Mass Transf 2006;128:240–50.
[28] Kuznetsov AV, Nield DA. Natural convective boundary-layer flow of a nanofluid past a vertical plate. Int J Ther Sci 2010;49:243–7.
[29] Khan WA, Pop I. Boundary-layer flow of a nanofluid past a stretching sheet. Int J Heat Mass Trans 2010;53:2477–83.
[30] Turkyilmazoglu M. Exact analytical solutions for heat and mass transfer of MHD slip flow in nanofluids. Chem Eng Sci 2012;84:182–7.
[31] Makinde OD, Khan WA, Khan ZH. Buoyancy effects on MHD stagnation point flow and heat transfer of a nanofluid past a convectively heated stretching/shrinking sheet. Int J Heat Mass Trans 2013;62:526–33.
[32] Rashidi MM, Abelman S, Mehr NF. Entropy generation in steady MHD flow due to a rotating porous disk in a nanofluid. Int J Heat Mass Trans 2013;62:515–25.
[33] Mustafa M, Farooq MA, Hayat T, Alsaedi A. Numerical and series solutions for stagnation point flow of nanofluid over an exponentially stretching sheet. PLoS ONE 2013;8:e61859.
[34] Sheikholeslami M, Ganji DD. Heat transfer of Cu-water nanofluid flow between parallel plates. Powder Tech 2013;235:873–9.
[35] Kuznetsov AV, Nield DA. Natural convective boundary-layer flow of a nanofluid past a vertical plate: a revised model. Int J Therm Sci 2014;77:126–9.
[36] Ramzan M, Bilal M. Time dependent MHD nano-second grade fluid flow induced by permeable vertical sheet with mixed convection and thermal radiation. PLoS ONE 2015;10(5):e0124929.
[37] Hayat T, Muhammad T, Alsaedi A, Alhuthali MS. Magnetohydrodynamic three-dimensional flow of viscoelastic nanofluid in the presence of nonlinear thermal radiation. J Mag Mag Mater 2015;385:222–9.
[38] Hayat T, Muhammad T, Qayyum A, Alsaedi A, Mustafa M. On squeezing flow of nanofluid in the presence of magneticfield effects. J Mol Liq 2016;213:179–85.
[39] Hayat T, Aziz A, Muhammad T, Alsaedi A, Mustafa M. On magnetohydrodynamic flow of second grade nanofluid over a convectively heated nonlinear stretching surface. Adv Powder Tech 2016;27:1992–2004.
[40] Hayat T, Aziz A, Muhammad T, Alsaedi A. On magnetohydrodynamic three-dimensional flow of nanofluid over a convectively heated nonlinear stretching surface. Int J Heat Mass Trans 2016;100:566–72.
[41] Hayat T, Muhammad T, Shehzad SA, Alsaedi A. An analytical solution for magnetohydrodynamic Oldroyd-B nanofluid flow induced by a stretching sheet with heat generation/absorption. Int J Ther Sci 2017;111:274–88.
[42] Akbarzadeh M, Rashidi S, Bovand M, Ellahi R. A sensitivity analysis on thermal and pumping power for the flow of nanofluid inside a wavy channel. J Mol Liq 2016;220:1–13.
[43] Sheikholeslami M, Ellahi R. Electrohydrodynamic nanofluid hydrothermal treatment in an enclosure with sinusoidal upper wall. Appl Sci 2015;5:294–306.
[44] Mamouriana M, Shirvan KM, Ellahi R, Rahimi AB. Optimization of mixed convection heat transfer with entropy generation in a wavy surface square lid-driven cavity by means of Taguchi approach. Int J Heat Mass Tranf 2016;102:544–54.
[45] Rahman SU, Ellahi R, Nadeem S, Zaigham Zia QM. Simultaneous effects of nanoparticles and slip on Jeffrey fluid through tapered artery with mild stenosis. J Mol Liq 2016;218:484–93.
[46] Liao SJ. On the homotopy analysis method for nonlinear problems. Appl Math Comput 2004;147(2):499–513.
[47] Wu B, Zhong H. Summation of perturbation solutions to nonlinear oscillations. Acta Mech 2002;154(1):121–7.
[48] Adomian G. A review of the decomposition method in applied mathematics. J Math Anal Appl 1988;135(2):501–44.
[49] He JH. Variational iteration method—a kind of non-linear analytical technique: some examples. Int J Non-Linear Mech 1999;34(4):699–708.
[50] Liao SJ. Homotopy analysis method: a new analytical technique for nonlinear problems. Commun Nonlinear Sci Numer Simul 1997;2(2):95–100.
[51] Liao SJ. An optimal homotopy-analysis approach for strongly nonlinear differential equations. Commun Nonlinear Sci Numer Simul 2010;15(8):2003–16.
[52] Farooq U, Zhao YL, Hayat T, Alsaedi A, Liao SJ. Application of the HAM-based Mathematica package BVPh 2.0 on MHD Falkner-Skan flow of nano-fluid. Comput Fluids 2015;111:69–75.
[53] Raees A, Xu H, Liao SJ. Unsteady mixed nano-bioconvection flow in a horizontal channel with its upper plate expanding or contracting. Int J Heat Mass Trans 2015;86:174–82.
[54] Nadeem S, Haq RU, Khan ZH. Numerical study of MHD boundary layer flow of a Maxwell fluid past a stretching sheet in the presence of nanoparticles. J Taiwan Inst Chem Eng 2014;45(1):121–6.
[55] Ishak A, Nazar R, Pop I. Heat transfer over an unsteady stretching permeable surface with prescribed wall temperature. Nonlinear Anal: Real World Appl 2009;10:2909–13.
[56] Hayat T, Qasim M, Mesloub S. MHD flow and heat transfer over permeable stretching sheet with slip conditions. Int J Numer Methods Fluids 2011;66:963–75.